Synthesis, Characterization, and Thermal Degradation of *p*-Chloroacetophenone Oxime Based Polymers Having Biological Activities

Narendra P. S. Chauhan,[1] Rakshit Ameta,[2] Suresh C. Ameta[1]

[1]*Department of Polymer Science, University College of Science, Mohan Lal Sukhadia University, Udaipur 313 001, Rajasthan, India*
[2]*Department of Pure and Applied Chemistry, University of Kota, Kota 324010, Rajasthan, India*

Received 11 September 2010; accepted 26 November 2010
DOI 10.1002/app.33966
Published online 4 May 2011 in Wiley Online Library (wileyonlinelibrary.com).

ABSTRACT: A monomer, *p*-chloroacetophenone oxime (CAO), has been synthesized from *p*-chloroacetophenone and hydroxylamine hydrochloride and its copolymer resin *p*-chloroacetophenone oxime-formaldehyde (CAO-F) has been synthesized from *p*-chloroacetophenone oxime (CAO) and formaldehyde in 1 : 2*M* proportion. A terpolymer resin *p*-chloroacetophenone oxime-formaldehyde-benzoic acid (CAO-F-BA) has also been synthesized by condensation of *p*-chloroacetophenone oxime (CAO), benzoic acid (BA), and formaldehyde (F) in 1 : 1 : 2*M* proportion in the presence of hydrochloric acid. The structures of monomer, copolymer, and terpolymer have been investigated by FT-IR, ^{1}H-NMR, and pyrolysis (GC/MS) techniques. Molecular weight and polydispersity index have been determined by gel permeation chromatography. Detailed thermal degradation studies of polymers have been carried out to ascertain its thermal stability. Multiple linear regression (MLR) method has been used to calculate activation energy (E_a) and frequency factor (Z). Thermodynamic parameters such as free energy (G^*), entropy change (ΔS^*), and rate constant for activation (k_r) have also been evaluated on the basis on Ozawa-Flynn-Wall method. Softening temperatures (T_s) of these resins have been obtained from differential scanning calorimetry (DSC). All the synthesized resins have shown reasonably good antimicrobial activities as compared to standard drugs. © 2011 Wiley Periodicals, Inc. J Appl Polym Sci 122: 573–585, 2011

Key words: *p*-chloroacetophenone oxime; pyrolysis (GC/MS); multiple linear regression (MLR); thermal degradation; thermoanalytical study; antimicrobial activity

INTRODUCTION

Polymer additives improve the manufacturing process and product quality. It can form continuous phase of coating with no deleterious effect on coating, and have better thermal stability.[1–5] Copolymer and terpolymer resins find quite useful applications as high temperature flame resistant fibers,[6] hardners,[7] ion exchange,[8] and semiconductors.[9] Yang and Sun[10] reported terpolymers of *N*-cyclohexylmaleimide methyl methacrylate and acrylonitrile by suspension polymerization. Katkamwar et al.[11] have prepared terpolymer resin from 8-hydroxyquinoline, dithiooxamide, and formaldehyde. Similarly, Gurnule et al.[12] synthesized terpolymer resins by condensation of 4-hydroxyacetophenone, biuret, and formaldehyde. Michael et al.[13] prepared terpolymer from 8-hydroxyquinoline, guanidine, and formaldehyde and also studied its thermal degradation to ascertain thermal stability. Gupta et al.[14] reported terpolymer resins by the condensation of 2-hydroxyacetophenone and melamine with formaldehyde. Hanes et al.[15] reported a series of anhydride-*co*-imide terpolymers based on trimellitylimido-L-tyrosine (TMA-Tyr), sebacic acid (SA), and 1,3-bis (carboxyphenoxy)propane (CPP) by melt condensation polymerization. Also, Fussell and Cooper[16] have studied the synthesis and characterization of acrylic terpolymer with RGD peptides for biomedical applications. Chauhan et al.[17] synthesized terpolymers based on *p*-hydroxybenzaldihyde oxime and also investigated their biological activities.

In the present article, we report the synthesis and characterization of a monomer, *p*-chloroacetophenone oxime, and its copolymer with formaldehyde and terpolymer with formaldehyde and benzoic acid. The structure, thermal, and biological properties of monomer CAO, copolymer CAO-F, and terpolymer CAO-F-BA were investigated. Their thermal degradation kinetics and thermodynamic parameters have also been discussed.

EXPERIMENTAL

Materials

p-chloroacetophenone and hydoxylamine hydrochloride were used as received from SRL, Mumbai.

Correspondence to: N. P. S. Chauhan (narendrapalsingh14@gmail.com).

Formaldehyde (37%) and benzoic acid were of analytical grade and chemically pure (all from Merck, India). Sodium hydroxide (Thomas Baker, Mumbai) was also used.

Instruments

FT-IR spectra of the polymer samples were recorded on Perkin–Elmer System-2000 (4000–400 cm^{-1}) spectrometer, using KBr pellet. ^{1}H-NMR spectra of polymer samples were taken in $CDCl_3$ on Bruker DPX-300 MHz NMR spectrometer. The internal reference used was tetramethylsilane (TMS). Pyrolysis GC/MS is assembled with GC (Autosystem XL) and MS (Perkin–Elmer Model Turbomass).

Gel permeation chromatography measurements were made for different resins soluble in tetrahydrofuran by Water Associates -200 Gel permeation chromatograph. The heart of the instrument is a series of columns, four feet long, 3/8 inches in diameter, packed with crosslinked polystyrene gel beads ($\sim$ 50 μm diameters). The porosity of gel beads is controlled by the amount of crosslinked agent (divinyl benzene) and also the amount and nature of diluents present during emulsion polymerization. Tetrahydrofuran was used as a solvent, stabilized with *t*-butylated hydroxytoluene (BHT) and served as mobile phase with flow rate of 2 mL/min.

A plot between weight loss and temperature was recorded in thermogravimetric analysis (TGA) using Pyris-1 (Perkin–Elmer, Shelton, USA). Initially, the sample (about 4 mg) was placed under nitrogen atmosphere (flow rate 20 mL/min); then the gas was changed to oxygen (flow rate 30 mL/min) and heating continued up to 800°C with heating rate at 25°C, 35°C, 45°C, and 55°C per minute. DTGA was performed at 25°C, which gives the decomposition temperature. Precision of temperature measurement was ±1.5°C.

Phase transitions were investigated over the range of 50–300°C in N_2 atmosphere using a Perkin–Elmer diamond differential scanning calorimetry (DSC). A plot between enthalpy change and temperature was obtained at heating rate of 10°C per minute.

Synthesis

Monomer [*p*-chloroacetophenone oxime (CAO)]

About 5.0 g of hydroxylamine hydrochloride was dissolved in 10.0 mL of water in a small conical flask and a solution of 3.0 g of sodium hydroxide in 10.0 mL of water was added. The solution was cooled in ice-cold water and 7.75 g of *p*-chloroacetophenone was added slowly. The flask was cooled, shaken well, and left overnight, when the oxime crystallized out. The crystals were filtered at the pump, dried rapidly between filter paper (yield = 3 g); melting point (90°C). IR (KBr, cm^{-1}): 3234, 2927, 1645, 1595, 1571, 1495, 1397, 1371, 1187, 929, 783, 747. ^{1}H-NMR [$CDCl_3$/TMS, (ppm)]: 11.34 (1H, s), 7.67 (2H, s), 7.45 (2H, s), 3.39 (3H, s), 2.13 (2H, s).

Copolymer [(*p*-chloroacetophenone oxime-formaldehyde (CAO-F)]

A mixture of monomer (*p*-chloroacetophenone oxime) (0.01 mol) and condensing reagent formaldehyde (0.02 mol) was taken in a round bottom flask. About 2.0 mL of 6.0*M* HCl was added slowly to the reaction mixture and the contents were refluxed at 60–80°C for 8–10 h on an oil bath with periodical shaking. After completion of the reaction, the mixture was poured in ice-cold water and washed with hot water to remove unreacted reactants. Finally, the product was washed with alcohol, dried in vacuum, and used for spectral analysis. IR (KBr, cm^{-1}): 3355, 2927, 1681, 1588, 1489, 1401, 1219, 1092, 1012, 840, 792, 762. ^{1}H-NMR [$CDCl_3$/TMS, (ppm)]: 7.15-7.75 (2H, m), 4.21-4.27 (2H, s), 3.24 (2H, s).

Terpolymer (*p*-chloroacetophenone oxime-formaldehyde-benzoic acid; CAO-F-BA)

A mixture of *p*-chloroacetophenone oxime (0.01 mol), condensing reagent formaldehyde (0.02 mol), and comonomer and benzoic acid (0.01 mol) was taken in a round bottom flask. About 2.0 mL of 6.0*M* HCl was added slowly to the reaction mixture and the contents were refluxed at 60–80°C for 8 to 10 h on an oil bath with occasional shaking to ensure thorough mixing. The separated terpolymer was washed with hot water and methanol to remove unreacted starting materials. The properly washed resin was dried and extracted with diethyl ether and then with petroleum ether to remove *p*-chloroacetophenone oxime-formaldehyde copolymer, which might be present along with *p*-chloroacetophenone oxime-formaldehyde-benzoic acid terpolymer. The brown-colored resinous product was immediately removed from the flask as soon as the reaction period was over. It was purified and then used for spectral characterization. IR (KBr, cm^{-1}): 3071, 2675, 2562, 1915, 1687, 1586, 1490, 1453, 1424, 1401, 1292, 934, 841, 810, 763. ^{1}H-NMR [$CDCl_3$/TMS, (ppm)]: 7.84 (3H, s), 7.15 (2H, dd), 4.18-4.42 (2H, s), 3.48 (2H, s).

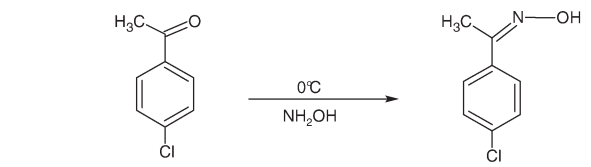

p-Chloroacetophenone oxime **(CAO)**

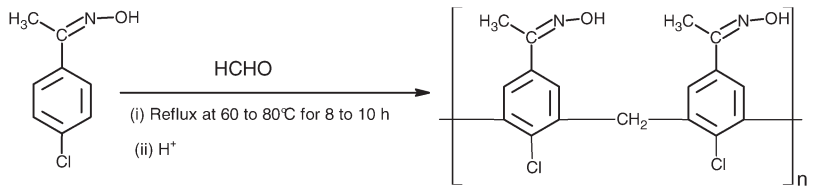

p-Chloroacetophenone oxime-formaldehyde **(CAO-F)**

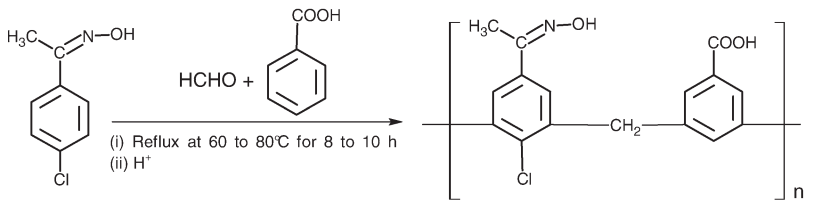

p-Chloroacetophenone oxime-formaldehyde-benzoic acid **(CAO-F-BA)**

Antibacterial activities

Pure cultures of pathogenic bacteria, viz., *Bacillus subtitlis*, *Escherichia coli*, *Staphylococus aureus*, *and Pseudomonas aeurginosa* were used for antibacterial activity. Cup or well method[18] was used for antibacterial studies. Nutrient agar medium was used for culture of the bacteria. The composition was beef-extract (3.0 g), peptones (5.0 g), sodium chloride (5.0 g), agar-agar (15.0 g), and distilled water (1000 mL). Nutrient agar medium was autoclaved at 15 psi and 121°C for 15 min. Sterilized petri dishes were placed in laminar flow bench. One end of the lid of each petri dish was lifted and approximately 15–20 mL of molten agar medium was poured into it and left for solidification. These were then inoculated with 0.2 mL suspension of organism by spread plate method. With the help of a sterile borer, six wells (five in periphery and one in center) were made in the medium and subsequently peripheral wells were filled with 500 ppm solution of the synthesized compound and the central well was filled with the standard drug used, i.e., ciprofloxacin at the same concentration. Other petri dishes were sealed with paraffin and incubated at 37°C in an incubator. The petri dishes were examined for zone of inhibition after 24–48 h. Concentrations of samples for antibacterial activity was taken as 500 μg/mL.

Antifungal activities

Pure cultures of pathogenic fungi, viz., *Alternaria solani* and *Fusarium oseyspurum* were used for antifungal activity studies. Antifungal activity of the extract was evaluated using poisoned food technique[19] on potato dextrose agar (PDA) medium. In this method, 20 mL of potato dextrose agar medium was poured in sterilized petri plates along with 1.0 mL of plant extract (1.0 mg/mL) and plated 6-mm diameters cups were removed from the center in which the same diameter mycelial discs (7-day-old culture) were inoculated. PDA medium without extract served as a control and the percent inhibition of mycelial growth was determined by the formula:

$$\text{Percent inhibition of mycelial growth} = \frac{C - T}{C} \times 100. \quad (1)$$

where C is average increase in mycelial growth in control plate and T is total increase in mycelial growth in treated plate. Concentration of samples for antifungal activity was taken as 500 μg/mL.

RESULTS AND DISCUSSION

Solubility

Solubility characteristics of resins were observed by using solvents of varying solubility parameters (Table I).

Spectral characterization

The molecular structures of CAO, CAO-F, and CAO-F-BA were established on the basis of FT-IR and ^{1}H-NMR data.

TABLE I
Solubility Characterstics of CAO, CAO-F, and CAO-F-BA

Solvent	CAO	CAO-F	CAO-F-BA
Benzene	Is	Is	Is
Toluene	S	S	S
Carbon disulphide	Is	Is	S
Acetone	Is	Is	Is
Ethanol	Is	Is	Is
Petroleum ether	Is	Is	Is
n-Hexane	Is	Is	Is
THF	S	S	S
DMSO	S	S	S
DMF	S	S	S
Chloroform	S	S	S
CCl_4	Is	Is	Is
NMP	S	S	S

The IR spectra of monomer, copolymer, and terpolymer are shown in Figure 1. In the range 3071–3355 cm^{-1}, a strong absorption band indicates the presence of OH stretching present in the oxime group. A lowest band in this range for terpolymer may be due to greater extent of H-bonding. A vibration band of methyl group appears near 2927 cm^{-1}. As the hydrogen bonded structure is stabilized by resonance, the OH stretching occurs as a broad band in the region 2562–2675 cm^{-1}. This clearly indicates that terpolymer has a greater extent of H bonding. Appearance of band ranging between 1645 and 1687 cm^{-1} is due to CO stretching in monomer, copolymer, and terpolymer. At 1489–1595 cm^{-1}, an intense band specific to the aromatic ring is also present. The peaks, characteristic of *para*-substituted benzene, are exhibited in the range of 745–792 cm^{-1}. The peak around 960 cm^{-1} is due to *N*—O stretching in oxime. The peak around 810 cm^{-1} is due to C—Cl stretching in monomer, copolymer, and terpolymer. Appearance of peak ranging from 1401–1453 cm^{-1} is due to bridged CH_2 group stretching of condensing reagent, which confirmed the structure of copolymer and terpolymer.

The ^{1}H-NMR spectra (Fig. 2) show a large broad signal centered in the range of 4.18–4.27 ppm. Appearance of these signals in copolymer (CAO-F) and terpolymer (CAO-F-BA) clearly indicates bridged —CH_2— group of condensing agent, which is absent in monomer (CAO). A sharp signal at 11.34 ppm is due to proton present in oxime group in CAO. This proton is free from H-bonding. In case of CAO-F and terpolymer CAO-F-BA, no signal appeared which might be due to high extent of H bonding. The signal that appears in the region between 7.14 and 7.84 ppm is due to aromatic ring protons present in CAO, CAO-F, and CAO-F-BA. The protons in the range of 3.24–3.48 ppm are due to protons of —$C(CH_3)$ (NOH) present in CAO, CAO-F, and CAO-F-BA.

Polymer degradation mechanism in pyrolysis (GC/MS)

The utility of this technique is based on the application of thermal energy to produce volatile fragments and products from a macromolecule or compounds capable of being analyzed using GC/MS.[20] The presence or absence of specific peaks in the pyrogram not only differentiates one sample from another but may be crucial in identifying defects related to product performance.[21] The degradation mechanisms experienced by polymers are free-radical processes initiated by bond dissociation at the pyrolysis temperature. The total ion chromatograms for pyrolysis of copolymer CAO-F and terpolymer CAO-F-BA (program are shown in Fig. 3) were identified by using the Willey and Nist library. For copolymer

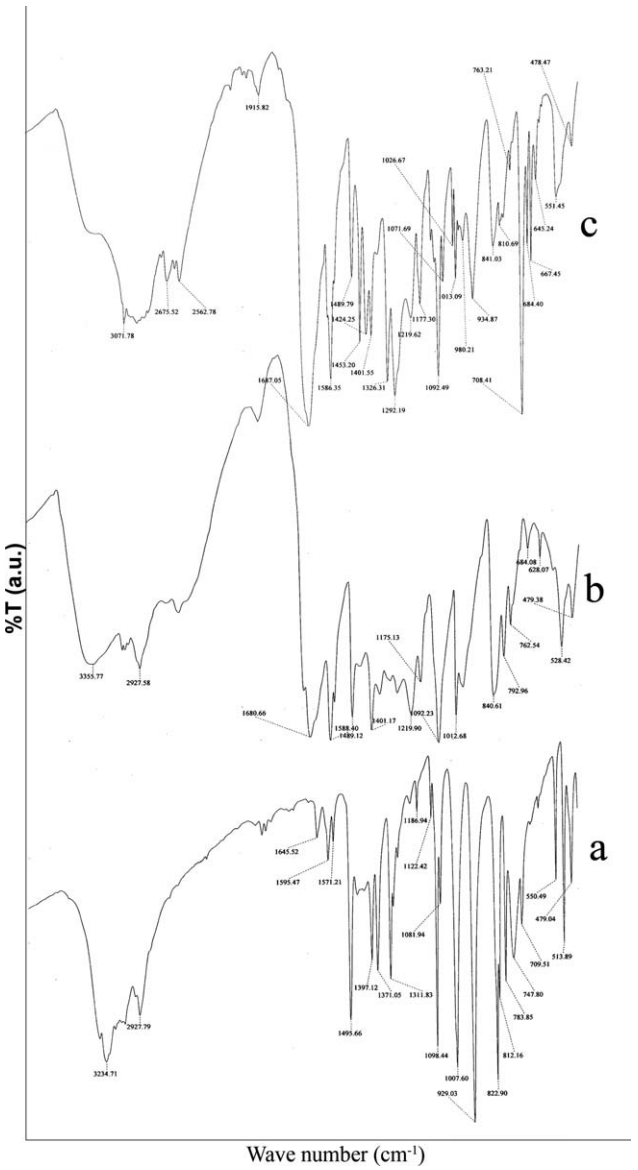

Figure 1 FT-IR spectra of (a) monomer CAO, (b) copolymer CAO-F, and (c) terpolymer CAO-F-BA.

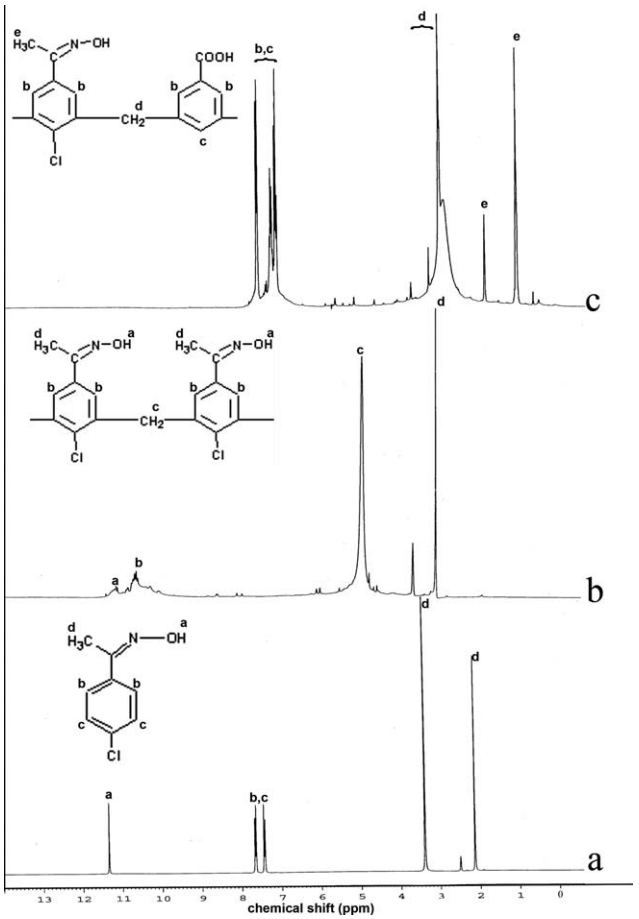

Figure 2 ^{1}H-NMR spectra of (a) monomer CAO, (b) copolymer CAO-F, and (c) terpolymer CAO-F-BA.

(CAO-F), there were three peaks in pyrogram, which may be due to 1-propanone, 1-(4-chlorophenyl)-(10.0), and bis(4-chlorophenyl)-methanone (8.56), and 1-chloro-3-methyl-benzene (4.0), whereas for terpolymer (CAO-F-BA), there were three large peaks in pyrogram, which may be due to monomer benzoic acid (9.18), 1-(4-chlorophenyl)-1-propanone (10.2), and 1-chloro-4-methyl-benzene (3.93).

These results indicate that pyrolysis mechanism may be due to random scission, unzipping, and side group elimination. In such polymers, pyrolysis gives either fragmentation to smaller oligomers units or unzipping to monomer. The groups attached to the side of the chain were held by bonds, which were weaker than the bonds connecting the chain. The side groups (oxime) are stripped off from the chain before it is broken into smaller pieces and hence, no monomer or higher oligomers were seen. A large number of unsolved peaks (1.03, 6.15, and 8.32) for terpolymer and (1.53 and 27.68) for copolymer may be due to side group scission kind of degradation mechanism. Nitrogen containing polymers usually generates some ammonia and hydrogen cyanide, and halogen containing polymers yield the respective hydrogen halide.[22] Similarly, In this case also, the chlorine removes hydrogen from polymer, making HCl gas. Pyrolysis produces either fragmentation to smaller oligomeric units or unzipping all the way to monomer in these polymers; however, the groups attached to the side of the chain are held by bonds connecting the chain. In such cases, the groups like oxime (=NOH), chloro (—Cl), and carboxylic acid (—COOH) stripped off from the chain before it is broken into smaller pieces. So no monomer or higher oligomers are seen. In halogen containing polymers, the carbon-chloride bond is the weakest and hence, a chlorine-free radical is generated at relatively low temperatures.

Molecular weights

The GPC fractionates a polymer sample on the basis of the molecular size. The interstitial volume of the column is accessible to all molecular species; the internal volume of the beads open to a particular species depends upon its size. The larger is the molecule, the smaller is the internal volume accessible to it. The smaller is the total volume (interstitial + internal) accessible to the molecule, the sooner it leaves the column. Thus, the largest molecule comes out first and the smallest the last. The data recorded by the instrument is a plot of retention volume versus refractive index difference ($R.I_{solution} - R.I_{solvent}$) i.e., differential distribution curve of the sample. With the

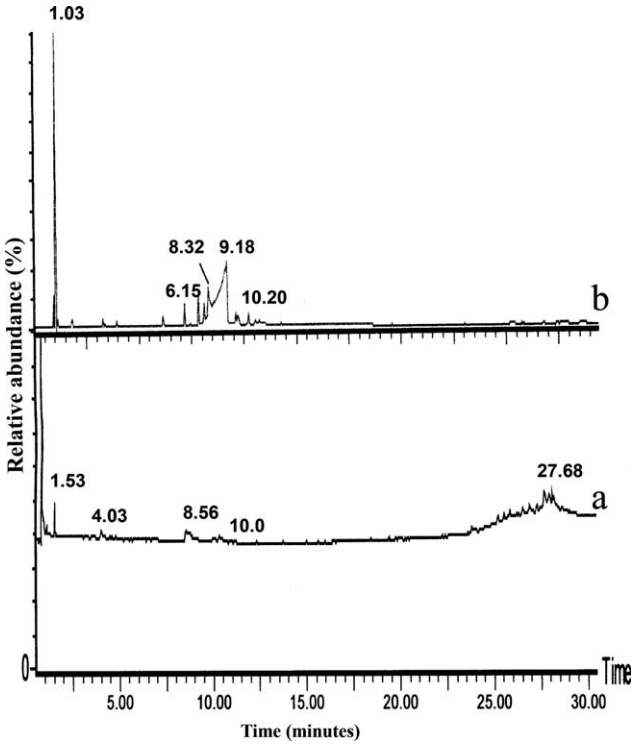

Figure 3 Total ion chromatogram obtained from pyrolysis of (a) copolymer CAO-F and (b) terpolymer CAO-F-BA.

TABLE II
GPC Data of Copolymer CAO-F, and Terpolymer CAO-F-BA

Code	$\overline{M}_n$ (g/mol)	$\overline{M}_w$ (g/mol)	$\overline{M}_z$ (g/mol)	Polydispersity index $\frac{\overline{M}_w}{\overline{M}_n}$	Starting molecular weight	Ending molecular weight
CAO-F	75	223	676	2.98	4825.8	2.5
CAO-F-BA	74	253	859	3.40	5316.4	2.1

help of this curve and a calibration curve, the average molecular weights of polymers under investigation were determined. The calibration curve was prepared with standard polystyrene samples of known molecular weight supplied by Water Associates.

For the computation of average molecular weights, the chromatogram was divided into vertical segments of equal elution volume. The height of each segment together with its corresponding molecular weight or molecular size, obtained from calibration curve, was used to calculate the molecular weights. The ratio of $\overline{M}_w$ to $\overline{M}_n$ gives the polydispersity index of the sample. It gives an idea of the lowest and highest molecular weight species as well as the distribution pattern of the intermediate molecular weight species. Polydispersity index for CAO-F is 2.98, which suggests that the present reaction proceeds through the polycondensation mechanism during formation of these polymers, whereas CAO-F-BA has an index of 3.4, which is formed from ionic (heterogeneous) polymerization. Different values of molecular weights and polydispersity indices are tabulated in Table II.

Starting and ending molecular weight is explained by the mechanism of the separation process. The starting molecular weight for large molecules, which occupy the greatest effective volume in solution, are excluded from the small pore sizes in the gel and pass quickly through the large channels between the gel particles. These results eluted first from the column. As the molecular size of the polymer decreases, there is an increasing probability that the molecules can diffuse into the smaller pores and channels in the gel, which slows down their time of passage through the column by providing a potentially longer path length for elution.

The starting molecular weight is referred for a large size of polymer molecule, whereas ending molecular weight for small size of polymers. The efficiency of the separation process is then a function of dependence of the retention (or elution) volume (V_R) on the molar mass (M), and a reliable relationship between the two parameters must be established. The value of (V_R) depends on the interstitial void volume (V_O) and the accessible part of the pore volume in the gel.

$$V_R = V_O + K_D V_i \tag{2}$$

where V_i is the total internal pore volume and K_D is the partition coefficient between V_i and the portion accessible to a given solute. Thus, $K_D = 0$ for very large molecules ($V_R = V_O$) and rapid elution takes place, whereas $K_D = 1$ for very small molecules, which can penetrate all the available pore volumes. This technique cannot discriminate among molecular sizes with $V_R \leq V_O$ or $V_R \geq V_O + V_i$.

For samples that fall within the appropriate range, it has been suggested that a universal calibration curve can be constructed to relate V_R and M, by assuming that the hydrodynamic volume of a macromolecule is related to the product $[\eta].M$, where $[\eta]$ is the intrinsic viscosity of the polymer in the carrier solvent used at the temperature of measurement. A calibration curve is then obtained by plotting log $[\eta].M$ against V_R for a given carrier solvent and at a fixed temperature.

The gel permeation chromatography (Figs. 4 and 5) clearly gives a narrow distribution of molecular framework and the PDI values, which indicates the mechanism to be polycondensation and ionic polymerization (heterogeneous) for copolymer (CAO-F) and terpolymer (CAO-F-BA), respectively.

TGA decomposition kinetics

The TGA scanning kinetic software program is based on the observations of Ozawa[23] and Flynn and Wall.[24] They noted that the activation energy of the thermal event can be directly determined from a series of TG runs performed at different rates. The mathematics show that if a series of TG runs is made at different scanning rates, each TG curve is shifted upward on the temperature scale with increasing scanning rates in such a way that a plot of the logarithm of the scanning rate vs. the inverse of the absolute temperature (at the same conversion or weight loss percentage) is linear, with a slope directly proportional to the activation energy and frequency factor. This state involves an approximation that has been discussed by Doyle[25] and by Flynn and Wall.[24] The approximation involves the so-called "exponential integral," which occurs in the theory, and methods of iteratively improving the results to a point of negligible error. Zsako et al.[26] proposed a closed form approximation for the exponential integral that is used in this program. The

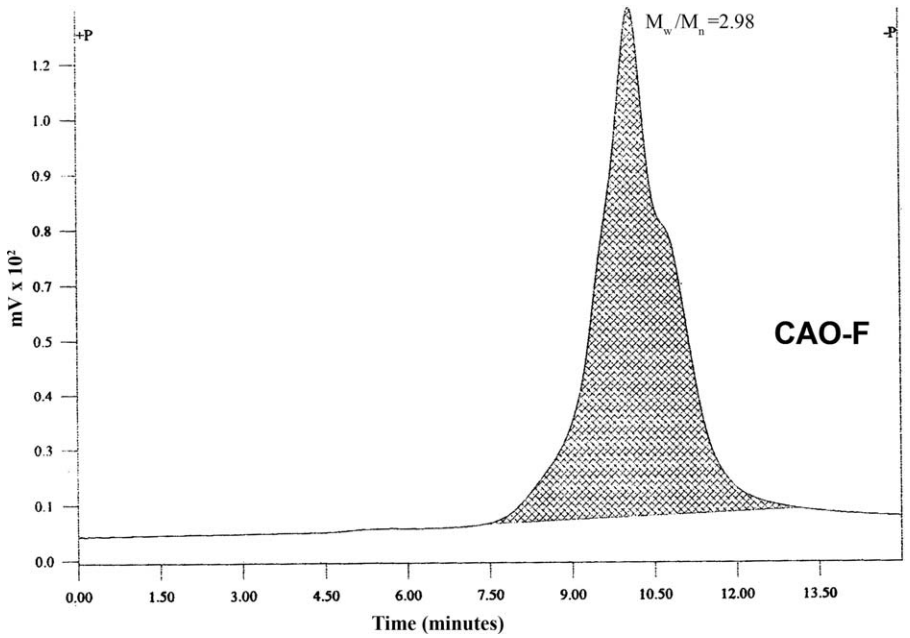

Figure 4 Gel permeation chromatogram for copolymer.

advantage of this method is that the activation energy is calculated absolutely independent of any assumptions concerning the dependence of the reaction rate on the percent reaction. The extension of this method to allow for nonunity reaction orders is also straight forward and utilizes the standard assumptions for *n*th order reaction kinetics.

The quality of the statistical fit can be judged from the 95% confidence limits and from observing the ln *r v/s* $1/T$ plot. In the ideal case, the data points fall on parallel straight lines, the slope of which is used to calculate the activation energy

Multiple linear regression (MLR) method

Using the standard method described, the activation energy and pre-exponential constants are calculated separately at each percent conversion, which has been used. When the MLR method is selected, the same percent conversion *vs*. temperature data are

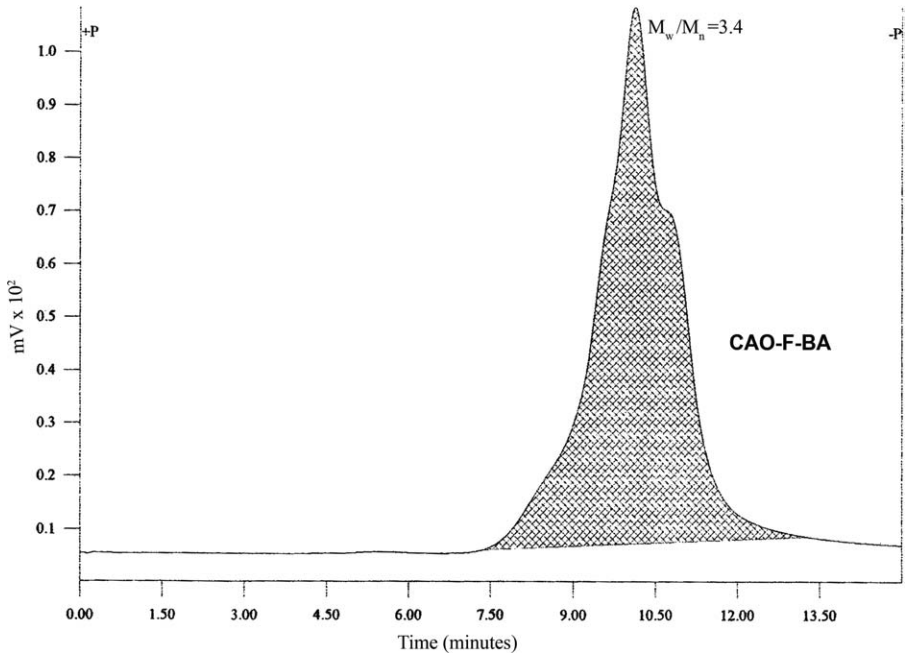

Figure 5 Gel permeation chromatogram for terpolymer.

TABLE III
Decomposition Kinetic Parameters of Copolymer CAO-F, and Terpolymer CAO-F-BA

	DTGA	TGA			
Code	Decomposition temperature at 25°C/min, T_d (K)	Activation energy (kJ/mol)	ln Z frequency factor (sec^{-1})	Z (sec^{-1})	Order of reaction
CAO-F	492	9	−4.3	0.02	1
CAO-F-BA	500	27	0.6	1.7	1

used. All the data are fitted to the same fundamental equations and a multilinear regression statistical treatment is used to find the value of the three kinetic parameters, which fit all the data best.

The MLR method has advantage that it is fitting a larger number of data points and, therefore, it is capable of giving better statistical results from a smaller number of experiments. Sometimes, if the data is noisier, it will only be possible to perform the MLR method.

A solid material is considered to be undergoing thermal decomposition according to the reaction.

$$A \xrightarrow{k} B + \Delta H$$

where A is the material before conversion, B is the material after conversion, k is the reaction rate, and ΔH is the heat of physical transition or heat of chemical reaction. In the chemical kinetic calculation, one is interested in the rate of change of A with time and its relation with temperature. If the decomposition starts at a temperature T_o and it is carried out by thermogravimetry at a linearly increasing temperature, then

$$T = T_o + rt \tag{3}$$

where r is the constant heating rate ($r = dT/dt$).

In thermogravimetric analysis, the conversion rate of the reaction may be defined as the ratio of actual mass loss to the total mass loss corresponding to the degradation process.

$$\alpha = \frac{M_o - M}{M_o - M_f} \tag{4}$$

where M, M_o, and M_f are the actual, initial, and final masses of the sample, respectively.

The rate of degradation ($d\alpha/dz$) can be expressed as functions of temperature and mass of the sample as

$$\frac{d\alpha}{dt} = A \exp\left(-\frac{E_a}{RT}\right)(1 - \alpha)^n \tag{5}$$

where A is the frequency factor, n is the reaction order, E_a is the apparent activation energy of the degradation reaction, R is the gas constant, and T is the absolute temperature. Upon introducing the heating rate, $r = (dT/dt)$, eq. (5) can be modified to

$$\frac{d\alpha}{(1 - \alpha)^n} = \frac{A}{r} \exp\left(-\frac{E_a}{RT}\right) dT \tag{6}$$

Therefore, eq. (6) is the fundamental relationship to determine kinetic parameters on the basis of TG data. The integral form of eq. (5) can be written as

$$g(\alpha) = \frac{A}{r} \int_0^T \exp\left(-\frac{E_a}{RT}\right) dT = \frac{AE_a}{rR} p(x) \tag{7}$$

where $x = \frac{E_a}{RT}$ and $p(x) = -\int_{\infty}^{\frac{E_a}{Rx}} \exp(-x)/x^2 dx$.

To describe the thermal degradation kinetics, Ozawa assumed log $p(x)$ ($-2.315 - 0.457x$ or ln p(x) ($-5.330 - 1.052x$ for $20 < x < 60$ for the nonplateau region of the curves. eq. (7) can be written as

$$\ln g(\alpha) = \ln \frac{AE_a}{rR} - 5.330 - 1.052 \frac{E_a}{RT} \tag{8}$$

Here, A and R are constants and, for a particular α or mass loss percentage, g(α) is a constant. Then eq. (8) becomes

$$\ln r = C - 1.052 \frac{E_a}{RT} \tag{9}$$

where the constant C is given by

$$C = \ln \frac{AE_a}{g(\alpha)R} - 5.330 \tag{10}$$

Hence, the value of E can be computed by Ozawa's method for any particular mass loss, being determined from the linear dependence of the ln r versus $1/T$ plot at different heating rates for the nonplateau region of the curves.

Decomposition kinetic parameters like activation energy, frequency factor, and order of reaction were determined by the MLR method. These kinetic parameters are tabulated in Table III. Both CAO-F and CAO-F-BA resins exhibit a three stage decomposition process. The first stage decomposition starts at 150°C, which may be due to removal of

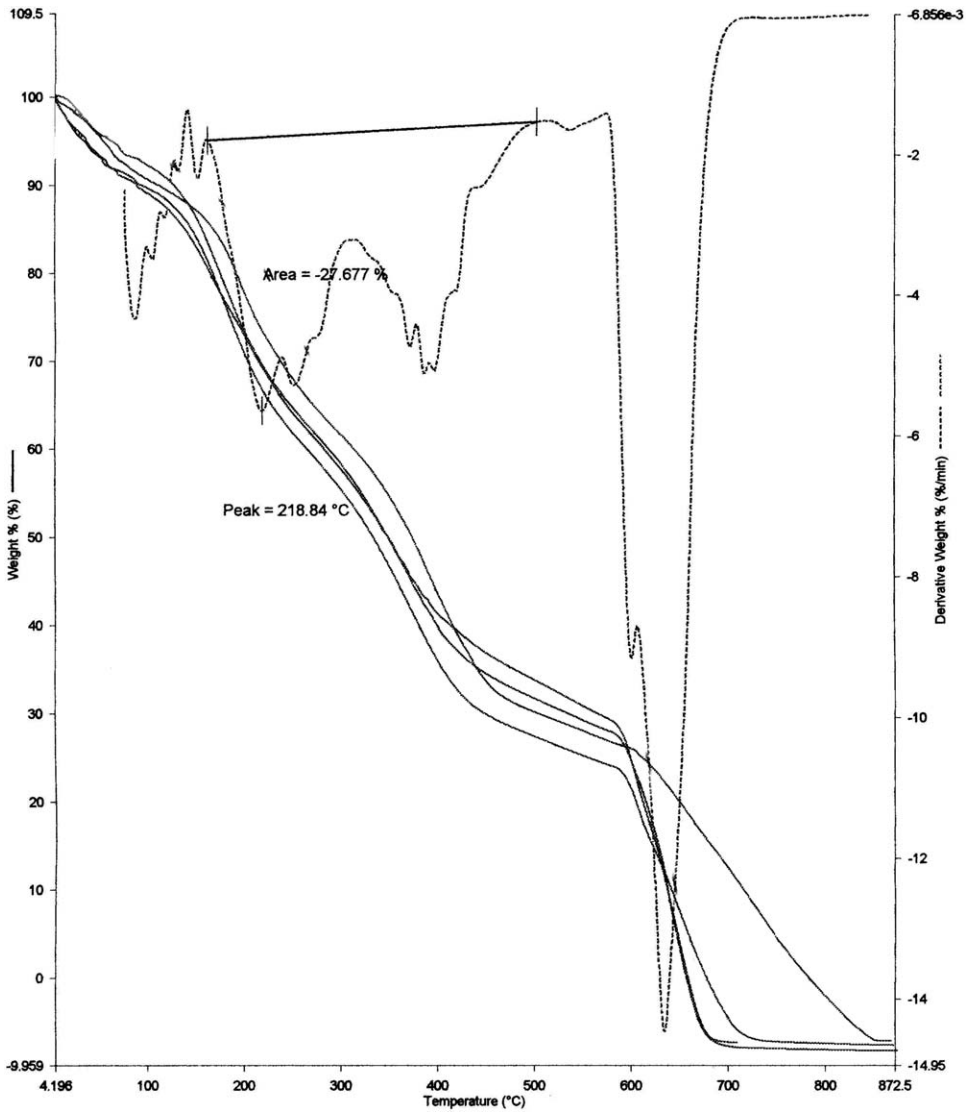

Figure 6 TGA at different scanning rates 25°C, 35°C, 45°C, and 55°C per minute and DTGA at 25°C for copolymer CAO-F.

carboxylic group (—COOH) present in the terpolymer as CO_2. In the second stage, the decomposition starts at 230°C and end up at 450°C, which corresponds to the loss of side chain attached to the aromatic nucleus. Third stage of decomposition starts at 450°C and the copolymer decomposes at 713°C whereas terpolymer at 778°C involves weight loss of around 98%. Terpolymer CAO-F-BA has higher decomposition temperature ($T_d = 500$ K, $E_a =$ 27 kJ/mol) than copolymer CAO-F ($T_d = 492$ K, $E_a = 9$ kJ/mol), which may be due to higher extent of H bonding (Figs. 6 and 7).

Thermodynamic parameters

By using data of thermogravimetric analysis, thermodynamic parameters[27] like apparent entopy change (ΔS^*), free energy of activation (G^*), and reaction rate of activation (k_r) have been determined on the basis of thermal degradation kinetics using eqs. (11)–(13):

(i) Entropy of activation (ΔS^*)

$$\Delta S^* = 2.303\ R \log \frac{Zh}{KT_s} \tag{11}$$

Where K is Boltzmann constant, h is Planck constant, and T_s is the peak temperature from DTGA.

(ii) Free energy of activation (G^*)

$$G^* = E^* - T\Delta S^* \tag{12}$$

(iii) Reaction rate constant for activation (k_r)

$$k_r = Ze^{-E^*/RT_s} \tag{13}$$

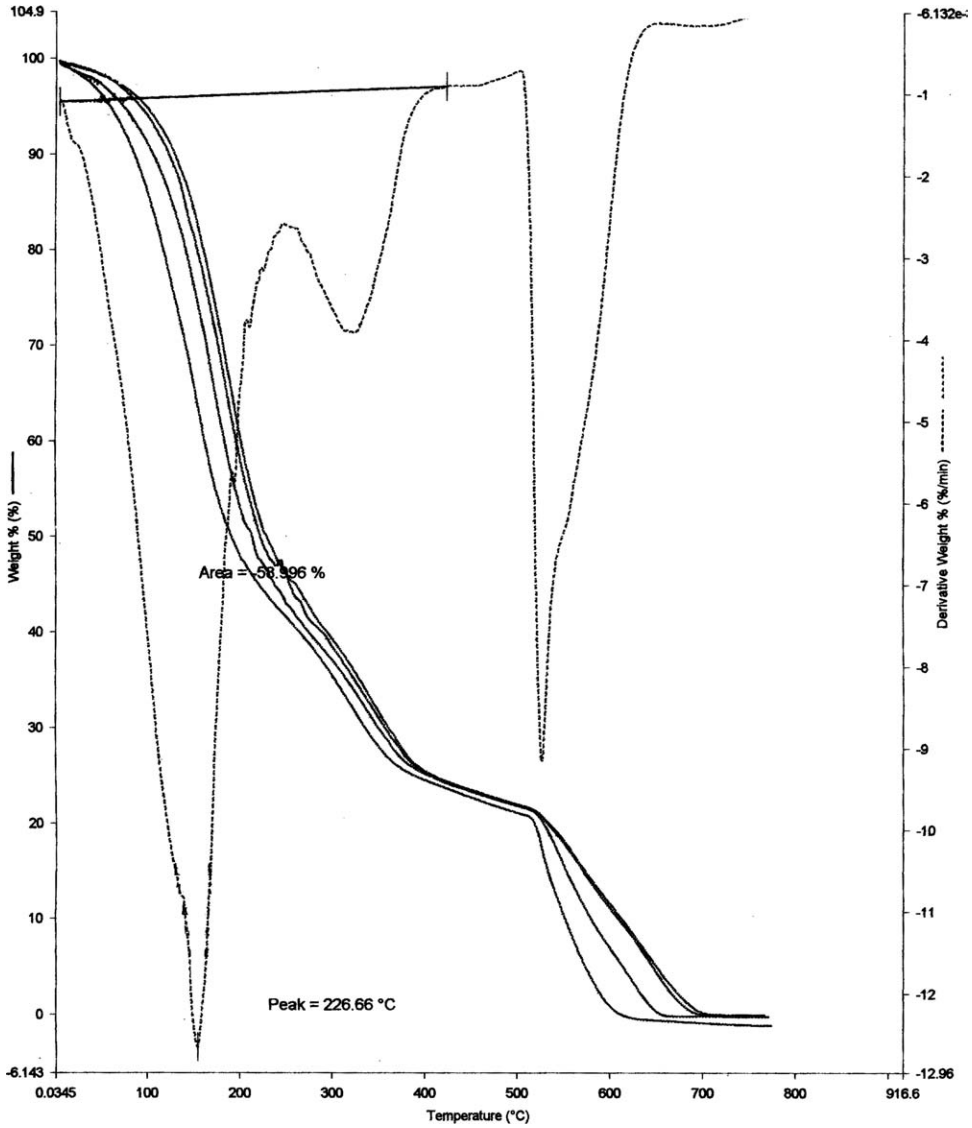

Figure 7 TGA at different scanning rates (25°C, 35°C, 45°C, and 55°C per minute) and DTGA at 25°C for terpolymer CAO-F-BA.

Thermodynamic parameters for copolymer APO-F and terpolymer APO-F-BA are tabulated Table IV. The negative value of DS* indicates that the activated complex has a more ordered structure than the reactants and further low values of Z indicate the slow nature of polymerization reaction.

Differential scanning calorimetry

The samples were heated at a rate of 10°C/min from 50 to 300°C. The plot shows the DSC heat flow as a function of sample temperature and endothermic response (heat absorbed by samples) is oriented toward the top of the graph. Softening point of CAO-F was observed at 96°C whereas it was obtained as 105°C for CAO-F-BA (Fig. 8). The heat of volatization for a number of polymers was measured by DSC where area under the endothermic peak was shown to be directly proportional to the heat of volatization. Heat of melting gives idea about percent crystallinty of polymers. CAO-F-BA shows maximum area under endothermic curve (422 mJ) and heat of melting (68 J/g) as compared to the endothermic curve (210 mJ) and heat of melting (34 J/g) for CAO-F.

Figure 8 shows that the endothermic response (heat absorbed by sample) is oriented toward the top of

TABLE IV
Thermodynamic Parameters of Copolymer CAO-F, and Terpolymer CAO-F-BA

Code	ΔS^* (kJ^{-1} $mol^{-1}K$)	G^* (kJ mol^{-1})	k_r (sec^{-1})
CAO-F	−85	51	1.4×10^{-3}
CAO-F-BA	−45	49	2.8×10^{-3}

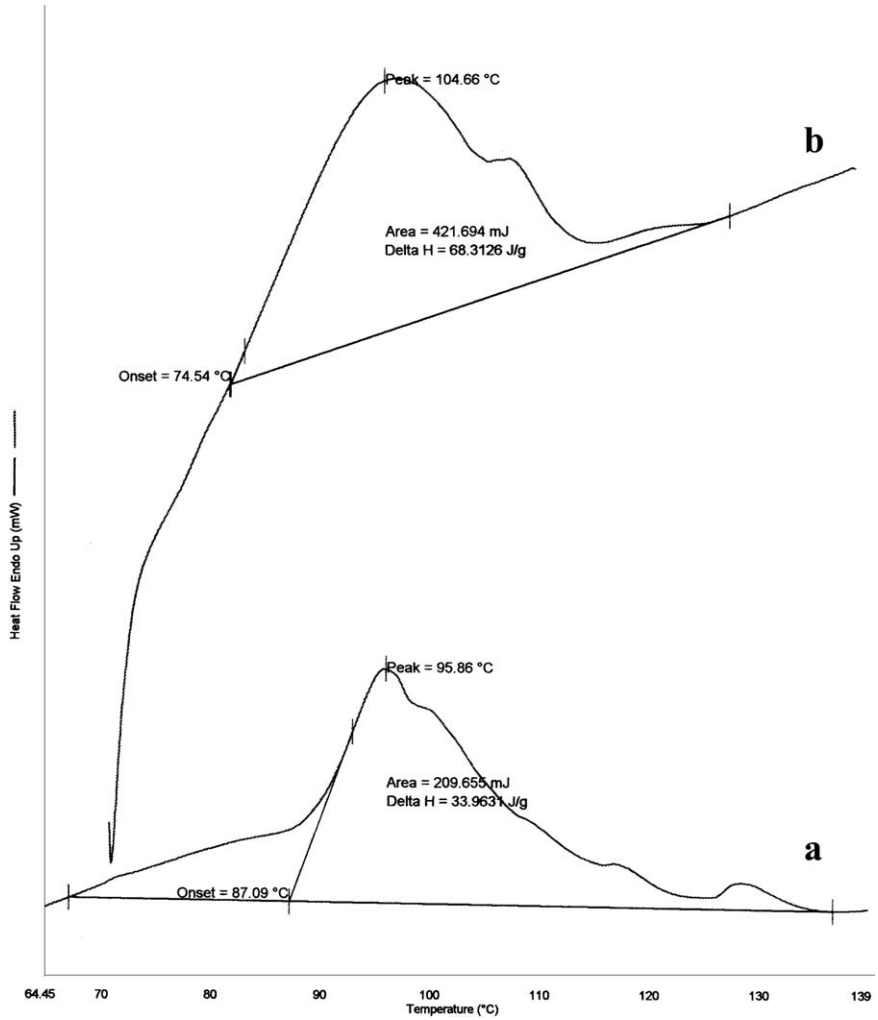

Figure 8 DSC scans of (a) copolymer CAO-F and (b) terpolymer CAO-F-BA.

the graphs. Softening temperatures of different copolymers and terpolymers are tabulated in Table V. The thermograms of copolymer CAO-F and terpolymer CAO-F-BA exhibit only one endotherm and two minor endotherms. The major endothermic peak at 105°C for CAO-F-BA is higher than the copolymer CAO-F (96°C), which may be due to a greater extent of H-bonding. These results are well in agreement apart from thermal (TGA) and spectroscopic observations (FT-IR and ^{1}H-NMR) described in the previous section. The presence of minor endotherms is attributed to the expulsion of water molecules loosely present in the polymer matrix. The thermograms also confirm the absence of any glass transition temperature for CAO-F and CAO-F-BA; the heat of volatization for a number of polymers was measured

TABLE V
DSC Thermogram Data of Copolymer CAO-F, and Terpolymer CAO-F-BA

Code	Onset temperature (T_o) (°C)	Softening temperature (T_s) (°C)	Area under endothermic peak (mJ)	Change in enthalpy (ΔH) (J/g)
CAO-F	87	96	210	34
CAO-F-BA	74	105	422	68

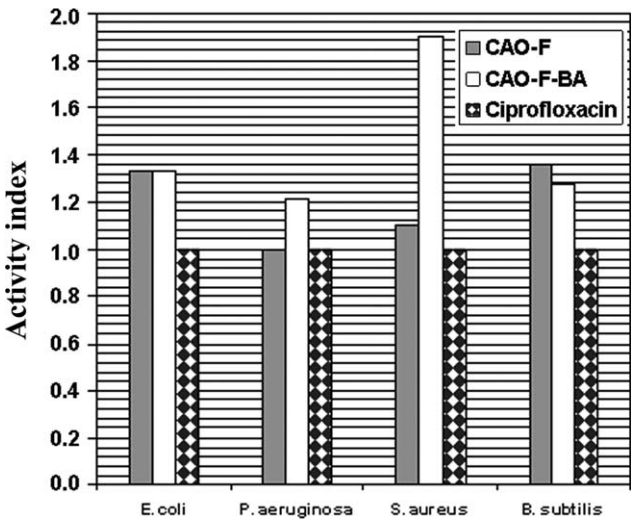

Figure 9 Comparative antibacterial activities of copolymer CAO-F, terpolymer CAO-F-BA, and standard drug.

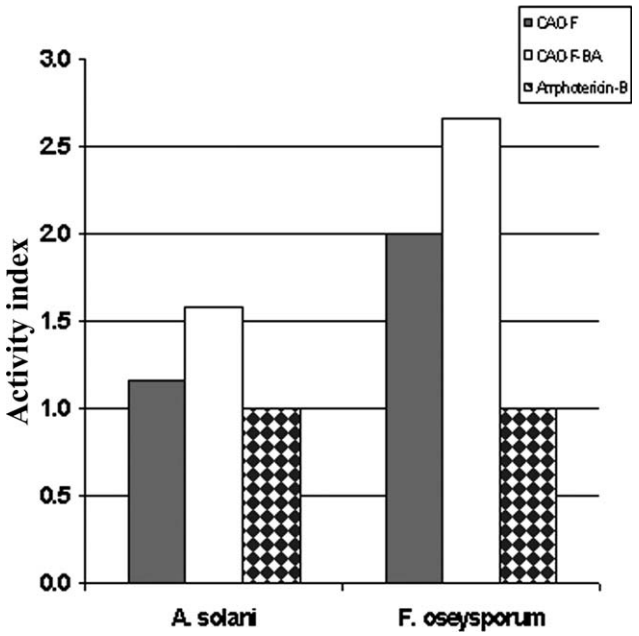

Figure 10 Comparative antifungal activities of copolymer CAO-F, terpolymer CAO-F-BA, and standard drug.

by DSC, where the area under the degradation endothermic peak was shown to be directly proportional to the heat of volatization for both.[28] Terpolymer CAO-F-BA has greater heat of volatization as compared to CAO-F which may be due to H-bonding (Table V).

Antimicrobial activity

To explore the antimicrobial properties, synthesized resins have been tested for their antibacterial activity against *Bacillus subtilis*, *Escherichia coli*, *Staphylococcus aureus*, and *Pseudomonas aeruginosa* and antifungal activity was observed against *Alternaria solani* and *Fusarium oseysporum*. Zone of inhibition and activity index with respect to standard antibacterial drug (ciprofloxacin) and standard antifungal drug (amphotericin-B) were measured (Fig. 9 for antibacterial activity and Fig. 10 for antifungal activity).

CAO-F and CAO-F-BA have shown good activity against all the bacteria and fungi used (Tables VI and VII). The CAO-F-BA has excellent antifungal and antibacterial activities as compared to CAO-F.

TABLE VI
Antibacterial Activity of Copolymer CAO-F, Terpolymer CAO-F-BA, and Ciprofloxacin

Code	Zone of inhibition in mm (activity index)			
	E. coli	*P. aeruginosa*	*S. aureus*	*B. subtilis*
CAO-F	16 (1.3)	14 (1.0)	11 (1.1)	15 (1.7)
CAO-F-BA	16 (1.3)	17 (1.2)	19 (1.9)	14 (1.3)
Standard drug (ciprofloxacin)	12 (1.0)	14 (1.0)	10 (1.0)	11 (1.0)

TABLE VII
Antifungal Activity of Copolymer CAO-F, Terpolymer CAO-F-BA, and Amphotericin-B

Code	Zone of inhibition in mm (activity index)	
	A. solani	*F. oseysporum*
CAO-F	14 (1.2)	12 (2.0)
CAO-F-BA	19 (1.6)	26 (2.7)
Standard drug (amphotericin-B)	12 (1.0)	06 (1.0)

CONCLUSIONS

Monomer (CAO), copolymer (CAO-F), and terpolymer (CAO-F-BA) have been easily prepared with high yields. FT-IR, ^{1}H-NMR, and pyrolysis GC/MS spectra were studied to elucidate the structures. Ozawa-Flynn-Wall method has been used to calculate activation energy (9 kJ/mol for CAO-F and 27 kJ/mol for CAO-F-BA). The TGA and DSC results revealed that the terpolymer has high thermal stability and softening temperature (105°C) as compared to the copolymer (96°C) which might be due to a larger extent of intramolecular H-bonding. Terpolymer CAO-F-BA required high activation energy as compared to copolymer CAO-F. These products can be used in the field of advanced materials. CAO-F-BA exhibit long-term antibacterial and antifungal properties. These materials, containing antimicrobial agents as oxime and the carboxyl group have been tested for their applicability to hospital product coatings.

Authors are thankful to HASETRI, JK Tyre, Rajsamand, CDRI, Lucknow, and SICART, Vallabh Vidyanagar, for analytical and spectral data of these samples.

References

1. Martina, O.; Werner, F.; Cristina, M. U.S. Patent 5705597-A.
2. Sauvet, G.; Dupond, S.; Kazmierski, K.; Chojnowski, J. Appl Polym Sci 2000, 75, 1005.
3. Singru, R. N.; Zade, A. B.; Gurnule, W. B. J Appl Polym Sci 2008, 109, 859.
4. Subramani, S.; Lee, J. M.; Lee, J. Y.; Kim, J. H. Polym Adv Technol 2007, 18, 601.
5. Ahmad, S.; Ashraf, S. M.; Sharmin, E.; Mohamad, A.; Alam, M. J Appl Polym Sci 2006, 100, 4981.
6. Eqorov, A. N.; Sukhorukov, Y. I.; Plotinkova, G. V.; Khaliullin, A.; Rus, K. J Appl Chem 2002, 75, 152.
7. Mustata, F.; Bicu, I. J Optoelect Adv Mat 2006, 8, 871.
8. Azarudeen, R. S.; Ahamed, M. A. R.; Jeyakumar, D.; Burkanudeen, A. B. Iran Polym J 2004, 18, 821.
9. Szabodka, O.; Varga, E.; Nagy, L. Talanta 2003, 59, 1081.
10. Yang, L.; Sun, D. J Appl Polym Sci 2007, 104, 792.
11. Katkamwar, S. S.; Zade, A. B.; Rahangdale, P. K.; Gurnule, W. B. J Appl Polym Sci 2009, 113, 3330.
12. Gurnule, W. B.; Rahangdale, P. K.; Paliwal, L. J.; Kharat, R. B. React Funct Polym 2003, 55, 255.
13. Michael, P. E. P.; Barbe, J. M.; Juneja, H. D.; Paliwal, L. J. Eur Polym Mater 2007, 43, 4995.

14. Gupta, R. H.; Zade, A. B.; Gurnule, W. B. J Appl Polym Sci 2008, 109, 3315.
15. Hanes, J; Chiba, M.; Langer, R. Macromolules 1996, 29, 5279.
16. Fussell, G. W.; Cooper, S. L. Biomaterials 2004, 25, 2971.
17. Chauhan, N. P. S.; Ameta, R.; Ameta, R.; Ameta, S. C. Malays Polym J 2010, 2, 162.
18. Black, J. G.; Schreiber, L. Microbiology: Principles and Explorations 4th ed.; Prentice Hall: New Jersey, 1999, p 363.
19. Collec, G. J.; Fraser, G. A.; Marmion, P. B.; Edinburgh, S. Practical Medical Microbiology, 14th ed.; Churchill Livingstone: Longman, Singapore, 1996; Vol. 11, p 163.
20. Acikqov, C.; Oney, O.; Kockar, O. M. J Anal App Pyrolysis 2004, 71, 417.
21. Scalarone, D.; Lazzari, M.; Chiantore, O. J Anal Appl Pyrolysis 2002, 64, 345.
22. Grassie, N.; Scott, G. Polymer Degradation and Stabilization; Cambridge University Press, Cambridge, 1985; pp 17–67.
23. Ozawa, T. J Therm Anal 1986, 31, 547.
24. Flynn, J. H.; Wall, L. A. Polym Lett 1966, 4, 323.
25. Doyle, C. D. Makromolekurae Chemie 1964, 80, 220.
26. Zsaka, J.; Varhelyi, M.; Varhelyi, C.; Liptay, G. Thermochim Acta 1981, 51, 277.
27. Yakuphaoglu, F.; Gorgulu, A. O.; Cukurovali, A. Physica B 2004, 353, 223.
28. Fredrick, W. J., Jr.; Mentzer, C. C. J Appl Polym Sci 1975, 19, 1799.